Sustainable Energy & Fuels

Improving levoglucosan and hydrocarbon production through gas-phase synergy during cellulose and polyolefin co-pyrolysis

Journal:	*Sustainable Energy & Fuels*
Manuscript ID	SE-ART-11-2021-001836.R1
Article Type:	Paper
Date Submitted by the Author:	28-Jan-2022

Complete List of Authors:	Xie, Shengyu; Tohoku University, Graduate School of Environmental Studies Ma, Chuan; Tohoku University, Graduate School of Environmental Studies Kumagai, Shogo; Tohoku University, Graduate School of Environmental Studies Takahashi, Yusuke; Tohoku University, Graduate School of Environmental Studies Kameda, Tomohito; Tohoku University, Saito, Yuko; Tohoku University Yoshioka, Toshiaki; Tohoku University, Graduate School of Environmental Studies

ARTICLE

Improving levoglucosan and hydrocarbon production through gas-phase synergy during cellulose and polyolefin co-pyrolysis†

Received 00th January 20xx,
Accepted 00th January 20xx

DOI: 10.1039/x0xx00000x

Shengyu Xie,[a] Chuan Ma,[a] Shogo Kumagai,[a,b,*] Yusuke Takahashi,[a] Tomohito Kameda,[a] Yuko Saito,[a] Toshiaki Yoshioka[a]

The co-pyrolysis of biomass and plastic is a promising technology for producing valuable chemicals. Herein, we report a novel split-flow tube reactor designed to focus on gas-phase synergy during the co-pyrolysis of cellulose and polyolefins, such as polyethylene (PE) and polypropylene (PP), at 650 °C in various blending proportions. The split-flow tube reactor significantly enhances levoglucosan (LG) recovery compared with the conventional straight-tube reactor, resulting in 3.1- and 2.1-times higher yields than those theoretically calculated (2.8 wt%) for 1:2 w/w cellulose/PE and 1:2 w/w cellulose/PP. In addition, gas-phase interactions between cellulose and polyolefin pyrolyzates were found to improve hydrocarbon-oil production by enhancing the decomposition of polyolefin-derived wax. These findings reveal that gas-phase pyrolytic interactions have significant potential for enhancing the production of chemical feedstocks or fuels from biomass and plastic waste.

1. Introduction

In recent years, renewable lignocellulosic biomass has replaced traditional fossil fuels for the production of platform chemicals and energy sources. Approximately 34 Mt (carbon equivalents) of biomass with high application potential was generated in Japan in 2015.[1] Furthermore, lignocellulosic biomass with carbon storage is gaining attention as a technology for meeting emission reduction targets set out in the Paris Agreement.[2] Pyrolysis technology can convert biomass into various by-products (oil, gas, and char) in the absence of reactive agents and has advantages that include short processing times and cost-effectiveness compared with biochemical conversion methods.[3]

Cellulose is a major component (40–50 wt%) of lignocellulosic biomass, the pyrolysis of which has been reported to yield anhydrosugars that are converted into low-molecular-weight products through dehydration and retro-aldol condensation.[4] Levoglucosan (LG), the main product from cellulose pyrolysis, has recently attracted widespread attention as a promising chemical platform; however, several parameters influence its recovery.[5] Gao et al.[6] found that low feedstock thickness (1 mm) and a high carrier-gas flow rate (>3 L/min) benefitted the production of LG during cellulose pyrolysis in a fixed-bed reactor because the rapid removal of volatiles minimizes secondary reactions. The recovery of LG is reportedly enhanced in a pyrolysis-gas chromatography/flame ionization detector (Py-GC/FID) system compared with a tube reactor due to rapid escape from the heating zone and low LG loading.[7] Acid-wash and Fenton pretreatment technologies have been developed to augment biomass pyrolysis, which led to increased LG yields owing to the disruption of the cellulose structure and the removal of alkaline earth metals.[8,9] In addition, some studies reported remarkably enhanced LG recoveries by the catalytic pyrolysis of biomass using metal and salt catalysts.[10,11]

Japan produced 8.9 Mt of plastic waste in 2018, of which 16% was sent to landfills or was incinerated, causing enormous carbon emission.[12] Some valuable chemicals and fuels from hard-to-recycle plastics can be recovered by thermochemical conversion.[13-16] Co-pyrolyzing biomass with plastic may solve issues associated with oil corrosion and instability resulting from high oxygen contents,[3] while further promoting the production of value-added chemicals through radical-reaction synergy.[17-19] In particular, polyolefins (PE: polyethylene; PP: polypropylene) account for half of the plastic waste production and contain a high hydrogen content; they can act as hydrogen donors to improve the pyrolytic reaction of hydrogen-deficient biomass.[20-22] A layered thin-film sample (PE at the top and cellulose at the bottom) was designed by Nallar et al., to increase the LG and hydrocarbon yields by inhibiting the escape of the cellulose pyrolyzate.[23] In our previous studies, beechwood pyrolysis in a PE melt at 350 °C was shown to deliver a 70% increase in LG yield because dispersing LG in the PE melt physically prevented its intermolecular condensation and ring-opening decomposition.[24] An enhanced polyolefin degradation was also observed during co-pyrolysis because of the presence of the oxygen-containing compounds from biomass.[25,26]

Various synergies between biomass and plastic further complicate the pyrolyzate distribution. Co-pyrolysis interactions compete in liquid/solid phases; the LG escape is suppressed and the polymerization is enhanced in the plastic melt, which decreases LG recovery.[23] At the same time, the acid-catalyzed ring opening of LG is inhibited because the melted plastic

[a] Graduate School of Environmental Studies, Tohoku University, 6-6-07 Aoba, Aramaki-aza, Aoba-ku, Sendai, Miyagi 980-8579, Japan. E-mail: kumagai@tohoku.ac.jp
[b] Division for the Establishment of Frontier Sciences of Organization for Advanced Studies, Tohoku University, 2-1-1 Katahira, Aoba-ku, Sendai 980-8577, Japan.

†Electronic Supplementary Information (ESI) available: See DOI: 10.1039/x0xx00000x

physically interferes with intermolecular proton transfer from other molecules.[24] In addition, the pore structure of biomass char fills the fused plastic, resulting in a delayed gas evolution.[27] LG fragmentation is inhibited in the gas phase owing to the abstraction of hydrogen from plastic pyrolyzates by LG radicals;[28] these gas-phase interactions also suppress pyrolyzate condensation and polymerization.[27] Therefore, the yields of the desirable products can be increased by controlling the synergistic interactions during cellulose and polyolefin co-pyrolysis, which not only maximizes the recovery of desired chemicals without any pretreatment or catalyst but also co-treats waste.

Herein, to elucidate the pyrolytic interactions in liquid/solid phase and in the gas phase during co-pyrolysis, the slow co-pyrolysis of cellulose and PE/PP at 650 °C was investigated by thermogravimetric analysis (TGA), evolved gas analysis-mass spectrometry (EGA-MS), and product-recovery tests by employing a straight-tube reactor (Fig. 1a). Slow heating is beneficial to evaluate the liquid-/solid-phase interactions owing to the diffusion barrier of the molten plastic. Furthermore, we designed a novel split-flow tube reactor (Fig. 1b) that focuses on the gas-phase synergy between cellulose and PE/PP pyrolyzates and effectively avoids liquid-/solid-phase interactions. The pyrolyzate distributions from the two types of reaction tubes (straight and split) were investigated and compared for a complete understanding of the synergy of co-pyrolysis and to maximize the recovery of desirable chemical feedstocks from biomass/plastic mixtures.

2. Materials and methods

2.1. Materials

Commercial cellulose, as well as low-density PE (average M_w = 4000) and PP (average M_w = 12000) were obtained from Sigma-Aldrich. The basic characterization of the cellulose sample is listed in Table S1 in the Electronic Supplementary Information (ESI). All materials were ground, sieved to 75–150 µm powders, and stored in a glass desiccator. Homogenous mixtures were prepared by homogenizing the cellulose and plastic samples in microtubes for 5 min at various blending ratios (Ce2PE1 and Ce1PE2 refer to 2:1 and 1:2 w/w cellulose/PE mixtures, respectively; similarly, Ce2PP1 and Ce1PP2 refer to 2:1 and 1:2 w/w cellulose/PP mixtures, respectively). The prepared raw materials were dried overnight at 105 °C to remove moisture prior to performing the experiment. Other chemicals and standard gases used in this study were purchased from Kanto Chemical (Tokyo, Japan) or Tokyo Chemical Industry (Tokyo, Japan).

2.2. Thermogravimetry

The thermal degradation behavior of the raw materials was examined by TGA (STA7200RV, Hitachi High-Tech Science Corporation, Japan). The samples (10 mg) loaded in a Pt pan were placed in the instrument, which was stabilized with nitrogen at 200 mL/min. The sample was then heated from 50 to 900 °C at 10 °C /min.

2.3. Pyrolysis in tube reactors

Pyrolysis experiments are performed in a horizontal quartz tube reactor (inner diameter: 7 mm) heated in an electric furnace, as shown in Fig. 1. A K-thermocouple was inserted from the furnace center, such that it touched the quartz tube; it fed the signal to the temperature controller. In the straight-tube reactor, a sample (0.1 g) was located at the furnace center and fixed in position with quartz wool. For the split-flow tube reactor, the cellulose and polyolefin samples (0.1 g of the total feedstock) were loaded in the two-branched quartz tube with a same inner diameter (7 mm). The junction of branched tubes was located at the furnace center. The temperature difference between the sample location and gas-phase junction was no greater than 5 °C. Other experimental conditions were identical for the two types of tube reactors. A helium (50 mL/min) sweep was allowed in the entire equipment during the pyrolysis test, to create an oxygen-free environment and to carry the pyrolyzates. The residence time of the carrier gas was 4.5 s in the heating zone throughout the experiments. Before heating, an aluminum bag was connected to the end of the device in order to collect gaseous products and a trap was placed in liquid nitrogen to collect liquid products. The furnace was then heated from ambient temperature to 650 °C at 10 °C/min. The heating was terminated after the furnace temperature was maintained at 650 °C for 30 min, and the tube reactor was naturally cooled to 50 °C with flowing helium. The cold trap was defrosted under continued helium flow to transfer the condensed gases into the aluminum bag. Each part was then separated, collected, and weighed. The quartz tube is cut into two sections and weighed according to product distribution: one part contains char while the other contains the liquid/solid condensate, as shown in Fig. S1 in the ESI. Super-dehydrated tetrahydrofuran (THF, 10 mL) was used to wash the cut tube, joint, and trap, and the THF-soluble products were collected. The pyrolysis experiment was repeated at least twice. The results were expressed as average values, and the experimental error was ≤5 %.

2.4. Product analysis

The recovered products consist of the following: (1) the char remaining in the heating zone, (2) liquid dissolved in THF, (3) solid THF-insoluble products (including coke from cellulose and wax from polyolefins) that condensed in the outer heating zone, and (4) gases collected in the aluminum bag. It should be noted that coke and wax were deposited in the same position of the reactor wall during the co-pyrolysis. Therefore, they were not independently quantified during the co-pyrolysis tests. A detailed analysis report is provided in the ESI. Briefly, the gas yield is the total amount of the identified gaseous products, and the liquid yield was calculated from the weight differences of the cut tube, joint, and trap before and after rinsing with THF. The specific gaseous and liquid pyrolyzates were identified and quantified by gas chromatography/mass spectrometry (GC/MS), gas chromatography with a thermal conductivity detector (GC/TCD), and gas chromatography with a flame ionization detector (GC/FID). In addition, a part of the liquid

needed to be pretreated by the oxime-trimethylsilylation (oxime-TMS) method to quantify LG, glycolaldehyde, and hydroxyacetone.[29] The yield of the solid was calculated from the weight difference of the THF-rinsed cut tube before and after combustion at 900 °C. The char yield was calculated from the weight difference of the cut tube before and after combustion at 900 °C. Thus, the mass balance was determined by the sum of gas, liquid, solid, and char yields.

2.5. *In-situ* pyrolyzate-monitoring by evolved gas analysis-mass spectrometry

Volatile compound behavior during pyrolysis was investigated by EGA-MS. The *in-situ* monitoring system consisted of a microfurnace pyrolyzer (EGA/PY-3030D, Frontier Laboratories, Japan) and an Agilent GC/MS system (GC: 6890; MS: 5975C; column: Ultra ALLOY deactivated metal capillary tube (UADTM, Frontier Laboratories, Japan)). Cellulose, polyolefin, or their mixtures (1 mg) were loaded into the holder and dropped into the furnace. The furnace was then heated from 50 to 650 °C at 10 °C/min. The evolved gases were rapidly swept into the GC/MS instrument. The residence time in the gas in the furnace was less than 0.1 s, which minimized secondary pyrolyzate reactions. The GC oven was maintained at 300 °C, the inlet temperature was set to 300 °C, and helium (1 mL/min) was used as the carrier gas with a 100:1 split ratio.

2.6. Identifying synergism

Cellulose/polyolefin synergy was investigated by comparing experimental results with those calculated theoretically according to Eq. 1:

$$Y_{mixture\_cal} = (1-\alpha)Y_{cellulose} + \alpha Y_{polyolefin} \quad (1),$$

where $Y_{mixture\_cal}$ is a theoretically calculated value (residual mass, mass-loss rate, pyrolyzate yield, or ion intensity), $Y_{cellulose}$ and $Y_{polyolefin}$ are the experimental values obtained by individually pyrolyzing cellulose and polyolefin, and α is the proportion of polyolefin in the mixture.

3. Results and Discussion

3.1. Co-pyrolysis of cellulose and polyolefins by direct contact mixing

3.1.1. Thermogravimetry

Fig. 2 shows TG and derivative TG (DTG) curves for various cellulose/polyolefin blending ratios, with characteristic data listed in Table 1. Cellulose mainly decomposes in the 300–400 °C temperature range, with a maximum mass-loss rate (30.6 wt%/min) observed at 348 °C. The cellulose produced 11.6 wt% char during pyrolysis at 650 °C. The PE degraded mainly at 400–500 °C, with a maximum mass-loss rate (23.2 wt%/min) observed at 477 °C, while PP had lower decomposition temperature (350–480 °C) than PE, with a maximum mass-loss rate (21.4 wt%/min at 457 °C). The DTG traces reveal that these plastics begin to decompose during the cellulose decomposition regime and that they are completely decomposed below 650 °C.

After co-pyrolysis, the residual mass of the mixture decreases with increasing polyolefin content. Furthermore, the rate of mass loss during the first stage decreases, while it increases in the second stage with increasing polyolefin blending proportion. The decomposition temperatures of cellulose and polyolefin affected each other when they were admixed. Cellulose was observed to decompose at a lower temperature than the theoretical TG- and DTG-calculated values, while the decomposition of PE or PP was delayed and began at a higher temperature. This phenomenon is also observed in the previous reports of biomass/polyolefins co-pyrolysis.[30,31] Cellulose devolatilization is accelerated in the presence of the plastic melt because the polyolefin (>0.15 W/(m·K)) is more thermally conductive than cellulose (0.04–0.05 W/(m·K)), which benefits heat transfer.[32,33] In addition, the fused polyolefin penetrates the pores of the less thermally conductive cellulose char [<0.08 W/(m·K)], which delays plastic decomposition.[27,34]

3.1.2. Pyrolyzate recovery from cellulose/polyolefin mixtures using the straight-tube reactor

The distributions of the products formed from cellulose, the polyolefins, and their mixtures in the straight-tube reactor are shown in Fig. 3. The cellulose pyrolysis products are primarily liquids (49.8 wt%) and solids (32.1 wt%) derived from anhydrosugar condensation and polymerization in the cold end of the tube. A lower gas yield (8.6 wt%) was obtained during slow pyrolysis, compared with that (34.3 wt%) observed during fast pyrolysis in a previous study at the same temperature[35] because a longer residence time increases the likelihood that the volatiles will recondense and polymerize.[36] Large amounts of solid are generated from the polyolefins due to wax formation. PP pyrolysis produced a high liquid yield (53.4 wt%) and a low solid yield (39.8 wt%) than PE (37.8 and 53.3 wt%, respectively). Lower gas and char yields were observed following co-pyrolysis and an increased amount of solid was formed with an increasing polyolefin ratio. A comparison of the experimental and theoretically calculated data reveals that synergistic interactions led to high liquid, gas, and char yields but low solid yields during cellulose/polyolefin co-pyrolysis.

The gaseous products obtained by the pyrolysis of cellulose alone mainly consist of CO (3.0 wt%) and CO_2 (5.2 wt%), as shown in Fig. 4. CO is produced by the decarbonylation of aldehydes, while CO_2 is mainly released during the early stage of cellulose pyrolysis.[37] C_2–C_4 hydrocarbons were the primary gaseous products of PE and PP pyrolysis because polyolefins only contain carbon and hydrogen. In particular, PP pyrolysis produced a higher yield (1.7 wt%) of C_3H_6 than other hydrocarbons. Significantly lower CO and CO_2 yields and higher gaseous hydrocarbon yields were obtained with an increasing polyolefin blending ratio. We also found that synergistic interactions in cellulose/polyolefin mixtures promote the production of CO and CO_2, with PE exhibiting a more significant enhancing effect than PP. In particular, the CO and CO_2 yields are 1.4- and 1.3-times higher than those calculated theoretically when the 2:1 cellulose/PE mixture was

pyrolyzed. These results are attributable to secondary decarbonylation and decarboxylation reactions, which are enhanced when the plastic melt acts as a physical barrier.[23]

Fig. 5 shows the yields of GC/MS-identified liquids produced by cellulose, the polyolefins, and their mixtures and excludes water and high-boiling-point compounds that are soluble in THF, which cannot be detected by GC. The detailed weight compositions of the identified pyrolyzates are listed in Tables S2 and S3. The tar produced by the pyrolysis of cellulose was found to mainly contain anhydrosugars (10.8 wt%). LG was produced in high yield (8.6 wt%) through chain reactions involving glycosidic bond cleavage and hydrolysis. The anhydrosugars occurred dehydration and ring-opening reactions and were further transformed into C_2–C_3 carbonyl compounds (2.1 wt%) by retro-aldol condensations or five-membered-ring compounds (0.2 wt%) by cyclization reactions.[38] The oil produced by polyolefin pyrolysis is classified as gasoline (C_5–C_{10}), kerosene (C_{11}–C_{13}), diesel (C_{14}–C_{18}), heavy gas oil (C_{19}–C_{25}), and C_{26+} hydrocarbons according to their oil properties.[39] Gasoline (2.6 wt%) was the dominant hydrocarbon fraction produced in PE pyrolysis (Fig 5a); in comparison, the PP pyrolysis afforded higher yields of each hydrocarbon fraction, with gasoline and diesel yields of 8.9 wt% and 6.2 wt%, respectively (Fig 5b). A co-pyrolysis led to relatively low yields of anhydrosugars and C_2–C_3 carbonyl compounds, with the hydrocarbon yield observed to increase with increasing PE/PP blend proportion. The LG yield produced during co-pyrolysis is higher than the theoretical values (5.7 vs. 7.8 wt%: cellulose/PE = 2:1; 2.8 vs. 4.8 wt%: cellulose/PE = 1:2). Higher LG yields (7.2 wt% and 3.8 wt%) were also observed following the co-pyrolysis of cellulose with PP (2:1 and 1:2). A higher char yield was observed under the same conditions, which is possibly due to the enhanced condensation of LG molecules by insufficiently dispersed cellulose in the polyolefin melt. Consequently, liquid-/solid-phase interactions negatively influence LG recovery under the present conditions. We conclude that the enhanced LG yield is the result of gas-phase pyrolytic interactions between LG and the pyrolyzates derived from the polyolefins. The LG in the liquid/solid phase evaporates and then cracks into C_2–C_3 carbonyl compounds and gases (CO, CO_2, and CH_4) by radical chain fragmentation with increasing pyrolysis temperature.[40] The LG radical is stabilized through gas-phase synergistic interactions involving hydrogen abstraction from hydrogen-rich polyolefin pyrolyzates, which suppresses the fragmentation and polymerization of LG.[28] Compared to theoretically calculated yields, lower C_2–C_3 carbonyl compound yields were obtained at a 2:1 cellulose/polyolefin ratio due to the inhibition of LG fragmentation. By contrast, the C_2–C_3 carbonyl compound yields obtained by pyrolysis of the 1:2 cellulose/polyolefin mixtures were not significantly lower than the theoretically calculated values because C_2–C_3 carbonyl compounds are produced through the degradation of anhydrosugar oligomers in the liquid/solid phase promoted by the longer residence time in the polyolefin melt. Furthermore, the gasoline yields obtained from the cellulose/polyolefin mixtures were lower, while the yields of the diesel, heavy gas oil, and C_{26+} fractions were higher than those calculated theoretically.

3.1.3. In-situ pyrolyzate-monitoring

The mass spectra of the volatiles obtained during cellulose, PE, and PP pyrolysis at various temperatures are shown in Fig. S2. The major peaks observed during cellulose pyrolysis at 300 °C correspond to gaseous products, including the molecular ions of H_2O (m/z = 18), CO (m/z = 28), and CO_2 (m/z = 44), which are derived from cellulose depolymerization.[41] Other peaks correspond polysaccharide pyrolyzate fragment ions, including LG (m/z = 57, 60, and 73), 1,6-anhydro-β-D-glucofuranose (m/z = 69, 73, and 85), levoglucosenone (m/z = 39, 68, 96, and 98), 1,4:3,6-dianhydro-α-D-glucopyranose (m/z = 29, 57, and 69), and 5-hydroxymethylfurfural (m/z = 39, 41, 69, 97, and 126). The peaks at m/z = 57, 60, and 73 were the most intense at 350 °C, which indicates that LG is produced in large quantities at this temperature. The m/z = 60 peak was less intense when the pyrolysis temperature was increased to 400 °C; the main ions observed at this temperature correspond to m/z = 28 and 44 (CO and CO_2) and result from LG decomposition.[42] The polyolefins exhibited peaks at m/z = 43, 57, and 71 corresponding to $C_3H_7^+$, $C_4H_9^+$, and $C_5H_{11}^+$ fragment ions at a pyrolysis temperature of 350 °C, and their intensities significantly increased at higher temperatures. These results supported the observation that the pyrolysis of polyolefins occurred at the same temperature range of cellulose pyrolysis, which verifies the feasibility of the gas-phase interactions at the current slow heating and is further enhanced with elevated temperature.

Fig. 6 shows the temperature-dependent product-emission behavior of cellulose, the polyolefins, and their mixtures. The total ion chromatograms (TICs) obtained by EGA-MS present similar results to those obtained by TGA. A comparison of the actual and theoretical curves reveals that the PE or PP melt accelerates the cellulose decomposition, and the formed cellulose char delays the polyolefin degradation. The peak at m/z = 18 corresponds to the molecular ion of H_2O derived from cellulose; this peak intensifies remarkably during co-pyrolysis, which indicates that the polyolefin promotes cellulose dehydration and anhydrosugar polymerization. The peak at m/z = 28 corresponds to the molecular ion of CO derived from cellulose and $C_2H_4^+$ produced by cellulose and the polyolefin; this peak mainly corresponds to CO at 300–375 °C. Moreover, the peak observed at m/z = 44 corresponds to the molecular ion of CO_2 from cellulose; both peaks (m/z = 28 and 44) were more intense after the addition of PE because the plastic melt promotes secondary reactions of cellulose pyrolyzates to produce more CO and CO_2. However, cellulose/PP interactions were found to influence the intensities of these peaks less than cellulose/PE interactions, consistent with the tube-reactor results. The peak at m/z = 60 corresponds to the major LG fragment ion; interestingly, this peak is less intense at a high polyolefin blending ratio than that predicted theoretically because the plastic melt physically aggravates LG polymerization.

3.2. Pyrolyzate recovery from cellulose/polyolefin mixtures using the split-flow tube reactor

As reported in the previous section, the TGA results revealed that the co-pyrolysis of cellulose and polyolefins altered their pyrolysis temperatures. In addition, the straight-tube reactor experiments and *in-situ* pyrolyzate-monitoring suggested that the diffusion barrier created by the molten plastic negatively impacted the recovery of LG and liquid hydrocarbons by favoring dehydration, decarbonylation, and decarboxylation reactions during cellulose pyrolysis. Therefore, this section employed a split-flow tube reactor that eliminates liquid-/solid-phase interactions to investigate the potential improvement of the recovery of target chemicals, such as levoglucosan and light hydrocarbons.

Fig 3 also shows the distributions of products obtained by pyrolyzing cellulose/polyolefin mixtures using the split-flow tube reactor. Higher liquid yields and lower gas and solid yields were obtained using this reactor than those obtained using the straight-tube reactor. Gas-phase interactions led to liquid yields that were enhanced by factors of 1.4, 1.5, 1.1, and 1.2 compared to the theoretically calculated values of Ce2PE1, Ce1PE2, Ce2PP1, and Ce1PP2 feedstocks, respectively. These results suggest that the gas-phase synergy between cellulose and polyolefin volatiles promotes the decomposition of coke/wax precursors into liquid fractions and decreases the risk of deposition in co-pyrolysis due to direct contact mixing.

Compared with the theoretically calculated values, gas-phase interactions during co-pyrolysis appear to inhibit CO and CO_2 formation more significantly with increasing PE or PP addition ratio (Fig. 4); this is attributable to the decomposition of vapor-phase LG into CO and CO_2. This decomposition is suppressed by the donation of hydrogen radicals from the plastic pyrolyzates.[28] In addition, the split-flow tube reactor produced lower yields of CO and CO_2 than the straight-tube reactor, which verified that the diffusion barrier of the plastic melt promotes the decarbonylation and decarboxylation reactions of cellulose in the liquid/solid phase, as shown in EGA-MS results.

Gas-phase interactions in the cellulose/polyolefin mixture during pyrolysis increase anhydrosugar production and decrease the yields of C_2–C_3 carbonyl compounds compared with the theoretically calculated values (Fig. 5). In particular, the split-flow tube reactor delivered LG yields that are 1.8-, 3.1-, 1.7-, and 2.1-times higher than the theoretically calculated values for Ce2PE1, Ce1PE2, Ce2PP1, and Ce1PP2, respectively, because the split-flow tube reactor eliminates the negative influence of liquid/solid interactions on LG recovery. LG radicals are stabilized by hydrogen abstraction from hydrogen-rich pyrolyzates formed from polyolefins in the gas phase, which suppresses LG fragmentation and condensation.[28] In addition, higher liquid-hydrocarbon yields of values 1.3-, 1.3-, 1.4-, and 1.2-times higher than the theoretically calculated values were obtained from the cellulose/PE (2:1 and 1:2) and cellulose/PP (2:1 and 1:2) mixtures through gas-phase interactions, which suggest that cellulose pyrolyzates promote the further decomposition of polyolefin pyrolyzates, as observed in fast co-pyrolysis experiments.[25,26]

Suggested pyrolysis pathways, which include synergistic interactions in the cellulose/polyolefin pyrolysis system, are shown in Fig. 7. Both liquid/solid-phase (Fig. 7(a)) and gas-phase (Fig. 7(b)) interactions occur in the straight-tube reactor. The escape of cellulose pyrolyzates is suppressed in the liquid/solid phase because the polyolefin melt physically prevents LG evaporation and promotes its decomposition into C_2-C_3 carbonyl compounds and small gaseous molecules.[23] The long residence time in the polyolefin melt also promotes LG polymerization, resulting in an enhanced char production. By contrast, the split-flow tube reactor eliminates liquid/solid-phase interactions; LG fragments into CO, CO_2, and C_2–C_3 carbonyl compounds through radical reactions in the gas phase.[40,43] The LG fragmentation is inhibited through H-abstraction from hydrogen-rich plastic pyrolyzates by LG radicals, which contributes to a higher LG yield and lower yields of CO, CO_2, and C_2–C_3 carbonyl compounds.[28] At the same time, the oxygen-containing compounds from cellulose pyrolysis promote the decomposition of the wax derived from polyolefins into hydrocarbon oil.[26,44]

4. Conclusions

Liquid-/solid-phase interactions between cellulose and polyolefins promote the production of CO, CO_2, and char during pyrolysis because the plastic melt acts as a physical barrier that suppresses the escape of cellulose pyrolyzates and promotes their decomposition and polymerization in the liquid/solid phase. The split-flow tube reactor eliminates the abovementioned negative pyrolytic interactions, resulting in the enhanced production of LG and hydrocarbon oil. The split-flow experiments delivered LG and hydrocarbon oil yields that are 3.1- and 1.3-times higher than the theoretically calculated values (2.8 and 5.1 wt%) for the 1:2 cellulose/PE mixture, and 2.1- and 1.2-times higher than theoretical yields (2.8 and 16.5 wt%) for the 1:2 cellulose/PP mixture, respectively. LG fragmentation is inhibited in the gas phase by H-abstraction from hydrogen-rich plastic pyrolyzates by LG radicals; radical reactions also accelerate the decomposition of high-molecular-weight wax into liquid hydrocarbons. Thus, the present results revealed the potential to further enhance gas-phase interactions under fast pyrolysis conditions, thus promoting LG and light hydrocarbon production. Although the potential of controlling pyrolytic interactions was confirmed in this work, a combination of real biomass and waste plastics must be investigated for their practical applications in the future.

Although the split-flow tube reactor was designed for validating the effectiveness of the gas-phase pyrolytic interactions in this work, the identified synergies in the gas phase have the potential to constitute a novel co-treatment process. In particular, plastic and biomass are independently fed into separate pyrolyzers, where they are pyrolyzed under appropriate conditions (temperature, feeding rate, and residential time). The volatiles are further reacted in the second pyrolyzer, where the yield and quality of high-value chemicals

or fuel can be maximized by controlling the pyrolytic interactions. The above-suggested approach is technologically feasible in the current industry. We believe that this work contributes to the effective utilization of waste plastics and biomass as carbon resources toward a circular economy and carbon neutrality in the future.

Author Contributions

Shengyu Xie: TGA and EGA-MS studies, data analysis, and manuscript drafting. **Chuan Ma:** Data analysis. **Shogo Kumagai:** conceptualization, supervision, and manuscript drafting. **Yusuke Takahashi**: Pyrolysis experiments using tube reactors, pyrolyzate analysis, **Tomohito Kameda, Yuko Saito, and Toshiaki Yoshioka:** drafting the introduction. All authors reviewed the manuscript.

Conflicts of interest

There are no conflicts to declare.

Acknowledgements

This work was supported by JSPS KAKENHI (Grant number: 19H04306) and the JST FOREST Program (Grant number: JPMJFR206U). Shengyu Xie was supported by the Chinese Scholarship Council (CSC).

References

1. *Wood Biomass Energy Data Book 2018*, Japan Woody Bioenergy Association, 2018.
2. Q. Yang, H. Zhou, P. Bartocci, F. Fantozzi, O. Mašek, F. A. Agblevor, Z. Wei, H. Yang, H. Chen, X. Lu, G. Chen, C. Zheng, C. P. Nielsen and M. B. McElroy, *Nat. Commun.*, 2021, **12**, 1698.
3. B. B. Uzoejinwa, X. He, S. Wang, A. El-Fatah Abomohra, Y. Hu and Q. Wang, *Energy Convers. Manage.*, 2018, **163**, 468-492.
4. S. Wang, G. Dai, H. Yang and Z. Luo, *Prog. Energy Combust. Sci.*, 2017, **62**, 33-86.
5. I. Itabaiana Junior, M. Avelar do Nascimento, R. O. M. A. de Souza, A. Dufour and R. Wojcieszak, *Green Chem.*, 2020, **22**, 5859-5880.
6. Z. Gao, N. Li, S. Yin and W. Yi, *Energy*, 2019, **175**, 1067-1074.
7. S. Kumagai, Y. Takahashi, T. Kameda, Y. Saito and T. Yoshioka, *ACS Omega*, 2021, **6**, 12022-12026.
8. S. Kumagai, R. Matsuno, G. Grause, T. Kameda and T. Yoshioka, *Bioresour. Technol.*, 2015, **178**, 76-82.
9. K. Wu, H. Wu, H. Zhang, B. Zhang, C. Wen, C. Hu, C. Liu and Q. Liu, *Waste Manage.*, 2020, **108**, 70-77.
10. X. Meng, H. Zhang, C. Liu and R. Xiao, *Energy Fuels*, 2016, **30**, 8369-8376.
11. G. F. David, S. d. P. S. Pereira, S. A. Fernandes, D. C. Cubides-Roman, R. K. Siqueira, V. H. Perez and V. Lacerda, *Waste Manage.*, 2021, **126**, 274-282.
12. *Plastic Waste Management Institute Newsletter*, 2020, **49**.
13. G. Lopez, M. Artetxe, M. Amutio, J. Bilbao and M. Olazar, *Renewable Sustainable Energy Rev.*, 2017, **73**, 346-368.
14. C. Wu and P. T. Williams, *Fuel*, 2010, **89**, 3022-3032.
15. C. Wang, H. Lei, M. Qian, E. Huo, Y. Zhao, Q. Zhang, W. Mateo, X. Lin, X. Kong, R. Zou and R. Ruan, *Sustainable Energy Fuels*, 2020, **4**, 4614-4624.
16. C. Ma, S. Kumagai, Y. Saito, T. Kameda and T. Yoshioka, *Green Chem.*, 2021, **23**, 6392-6404.
17. Z. Wang, K. G. Burra, T. Lei and A. K. Gupta, *Prog. Energy Combust. Sci.*, 2021, **84**, 100899.
18. D. K. Ojha and R. Vinu, *RSC Advances*, 2015, **5**, 66861-66870.
19. D. Duan, Y. Zhang, H. Lei, M. Qian, E. Villota, C. Wang, Y. Wang and R. Ruan, *Sustainable Energy Fuels*, 2020, **4**, 3687-3700.
20. S. Kumagai and T. Yoshioka, *Anal. Sci.*, 2021, **37**, 145-157.
21. G. Lopez, A. Erkiaga, M. Amutio, J. Bilbao and M. Olazar, *Fuel*, 2015, **153**, 393-401.
22. C. Ma, S. Xie, S. Kumagai, Y. Takahashi, Y. Saito, T. Kameda and T. Yoshioka, *Chem. Eng. J.*, 2022, **431**, 134030.
23. M. Nallar and H.-W. Wong, *ACS Sustainable Chem. Eng.*, 2019, **7**, 9480-9488.
24. S. Kumagai, K. Fujita, Y. Takahashi, Y. Nakai, T. Kameda, Y. Saito and T. Yoshioka, *Sci. Rep.*, 2019, **9**, 1955.
25. S. Xie, S. Kumagai, T. Kameda, Y. Saito and T. Yoshioka, *Bioresour. Technol.*, 2021, **337**, 125435.
26. K. Kasataka, S. Kumagai, T. Kameda, Y. Saito and T. Yoshioka, *Bioresour. Technol. Rep.*, 2020, **11**, 100431.
27. X. Liu, K. G. Burra, Z. Wang, J. Li, D. Che and A. K. Gupta, *Appl. Energy*, 2020, **279**, 115811.
28. S. Kumagai, K. Fujita, T. Kameda and T. Yoshioka, *J. Anal. Appl. Pyrolysis*, 2016, **122**, 531-540.
29. T. Hosoya, H. Kawamoto and S. Saka, *J. Anal. Appl. Pyrolysis*, 2006, **77**, 121-126.
30. E. Părpăriţă, M. T. Nistor, M.-C. Popescu and C. Vasile, *Polym. Degrad. Stab.*, 2014, **109**, 13-20.
31. Y. Wen, I. N. Zaini, S. Wang, W. Mu, P. G. Jönsson and W. Yang, *Energy*, 2021, **229**, 120693.
32. B. Petter Jelle, in *Start-Up Creation*, eds. F. Pacheco-Torgal, E. Rasmussen, C.-G. Granqvist, V. Ivanov, A. Kaklauskas and S. Makonin, Woodhead Publishing, 2016, pp. 129-181.
33. R. Klein, in *Laser welding of plastics: materials, processes and industrial applications*, John Wiley & Sons, 2012, ch. 1, pp. 3-69.
34. C. A. Koufopanos, N. Papayannakos, G. Maschio and A. Lucchesi, 1991, **69**, 907-915.
35. S. Kumagai, K. Fujita, Y. Takahashi, T. Kameda, Y. Saito and T. Yoshioka, *J. Jpn. Inst. Energy*, 2019, **98**, 202-219.
36. Q. M. K. Waheed, M. A. Nahil and P. T. Williams, *J. Energy Inst.*, 2013, **86**, 233-241.
37. S. Li, J. Lyons-Hart, J. Banyasz and K. Shafer, *Fuel*, 2001, **80**, 1809-1817.
38. R. Vinu and L. J. Broadbelt, *Energy Environ. Sci.*, 2012, **5**, 9808-9826.
39. R. C. Selley and S. A. Sonnenberg, in *Elements of Petroleum Geology (Third Edition)*, eds. R. C. Selley and S. A. Sonnenberg, Academic Press, Boston, 2015, ch. 2, pp. 13-39.
40. A. Fukutome, H. Kawamoto and S. Saka, *ChemSusChem*, 2015, **8**, 2240-2249.
41. S. D. Gunasee, M. Carrier, J. F. Gorgens and R. Mohee, *J. Anal. Appl. Pyrolysis*, 2016, **121**, 50-61.
42. R. J. Evans and T. A. Milne, *Energy Fuels*, 1987, **1**, 123-137.
43. T. Hosoya, H. Kawamoto and S. Saka, *J. Anal. Appl. Pyrolysis*, 2008, **83**, 64-70.
44. H. Yuan, H. Fan, R. Shan, M. He, J. Gu and Y. Chen, *Energy Convers. Manage.*, 2018, **157**, 517-526.

Table 1 Characteristic TG and DTG features for cellulose, PE, PP, and their mixtures

Sample	First stage				Second stage				Residue (wt%)	Residue_cal (wt%)
	T_{max1} (°C)	D_{max1} (wt%/min)	T_{max1}_cal (°C)	D_{max1}_cal (wt%/min)	T_{max2} (°C)	D_{max2} (wt%/min)	T_{max2}_cal (°C)	D_{max2}_cal (wt%/min)		
Cellulose	348	30.6	–	–	–	–	–	–	11.6	–
Ce2PE1	348	19.2	348	20.5	484	8.7	477	7.9	8.2	7.6
Ce1PE2	337	8.9	348	10.5	479	16.4	477	15.5	5.5	3.5
PE	–	–	–	–	477	23.2	–	–	0.0	–
Ce2PP1	348	19.5	349	20.7	470	7.4	457	7.3	8.4	7.9
Ce1PP2	339	7.9	349	10.8	465	16.5	457	14.4	4.9	4.1
PP	–	–	–	–	457	21.4	–	–	0.0	–

T_{max}: Maximum mass-loss-rate temperature; D_{max}: maximum mass-loss rate; T_{max}_cal: theoretically calculated maximum mass-loss-rate temperature; D_{max}_cal: theoretically calculated maximum mass-loss rate.

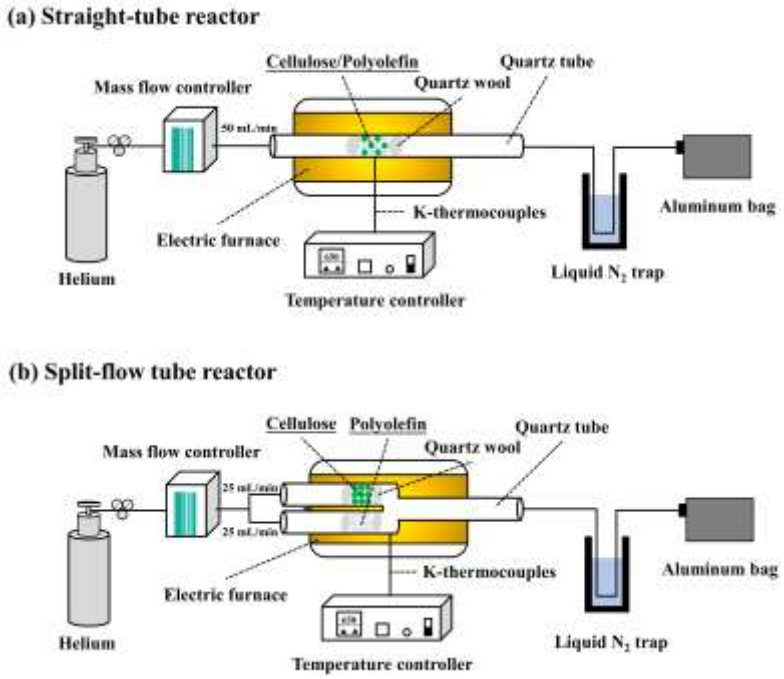

Fig. 1 Pyrolysis equipment: schematics of (a) the straight-tube reactor and (b) the split-flow tube reactor.

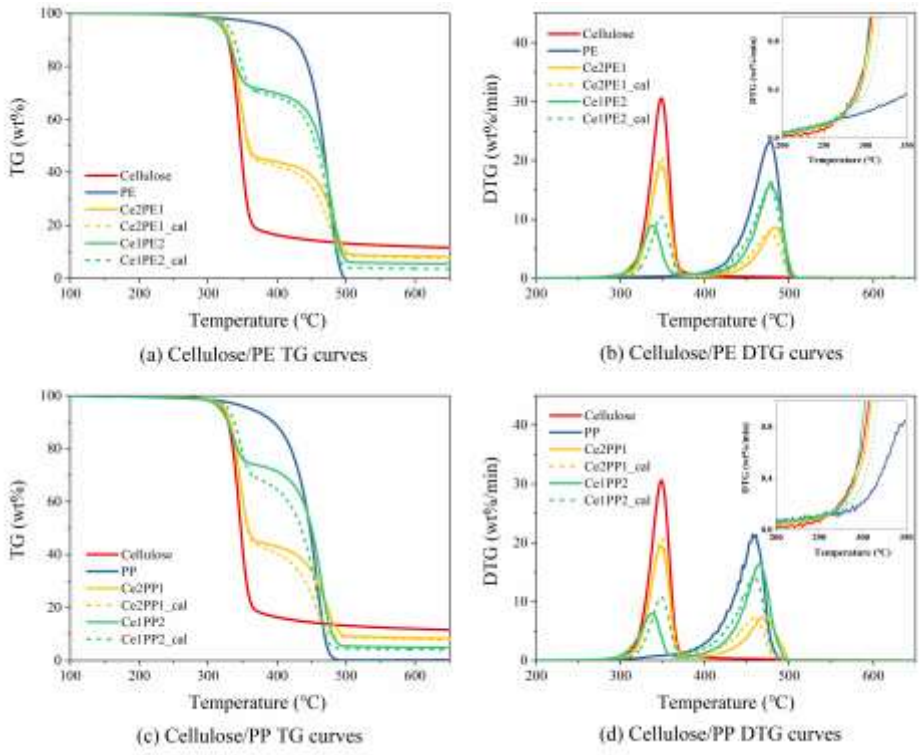

Fig. 2 (a, c) TG and (b, d) DTG curves obtained for various (a, b) cellulose/PE and (c, d) cellulose/PP blending ratios at 10 °C/min.

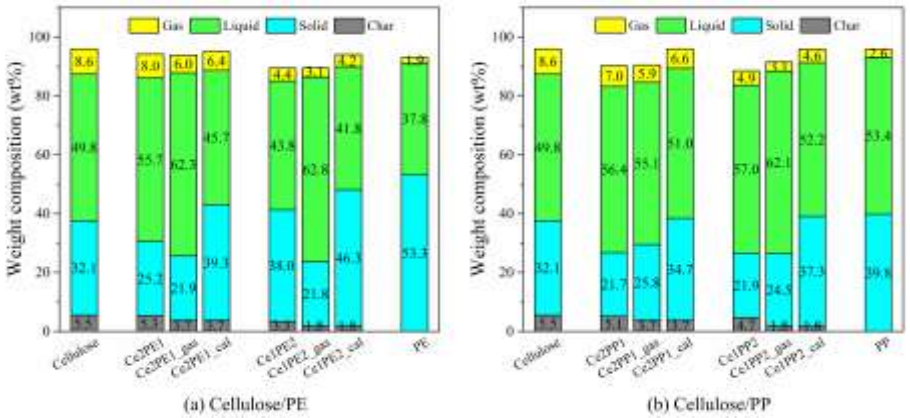

Fig. 3 Product weight compositions from cellulose and polyolefin co-pyrolysis in the two tube reactors: (a) cellulose/PE and (b) cellulose/PP; "_gas" refers to experiments performed in the split-flow tube reactor and "_cal" indicates theoretical yields calculated on the basis of the pyrolysis of neat cellulose and polyolefins.

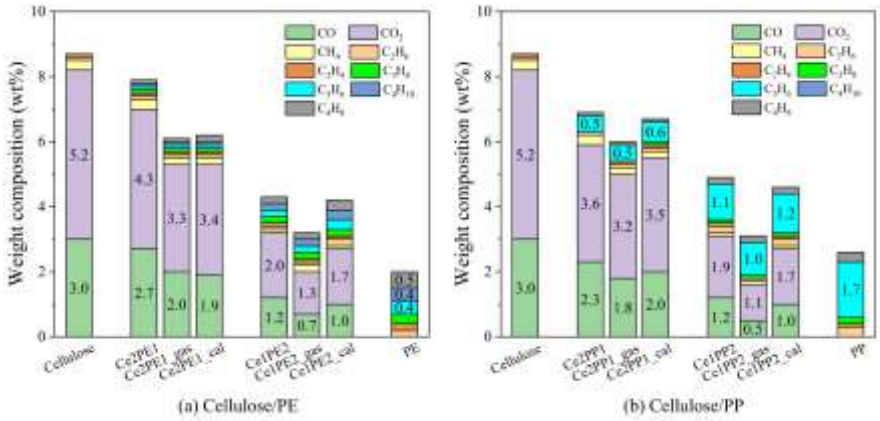

Fig. 4 Gaseous product yields from cellulose and polyolefin co-pyrolysis in the two tube reactors: (a) cellulose/PE and (b) cellulose/PP; "_gas" refers to experiments performed in the split-flow tube reactor and "_cal" indicates theoretical yields calculated on the basis of the pyrolysis of neat cellulose and polyolefins.

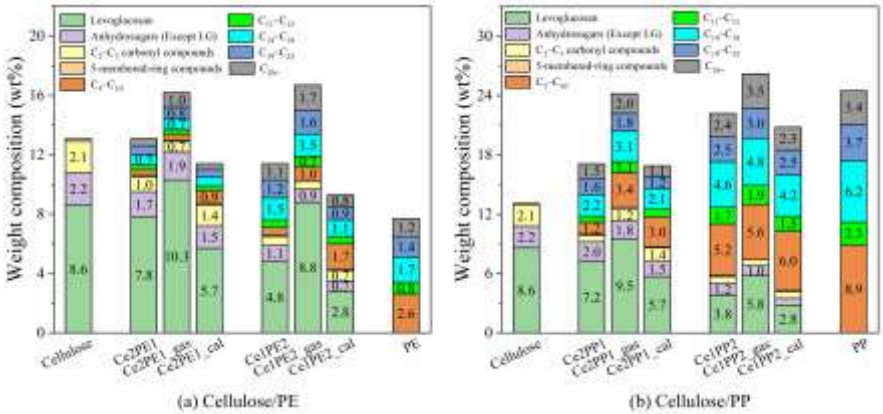

Fig. 5 Liquid product yields from cellulose and polyolefin co-pyrolysis in the two tube reactors: (a) cellulose/PE and (b) cellulose/PP; "_gas" refers to experiments performed in the split-flow tube reactor and "_cal" indicates theoretical yields calculated on the basis of the pyrolysis of neat cellulose and polyolefins.

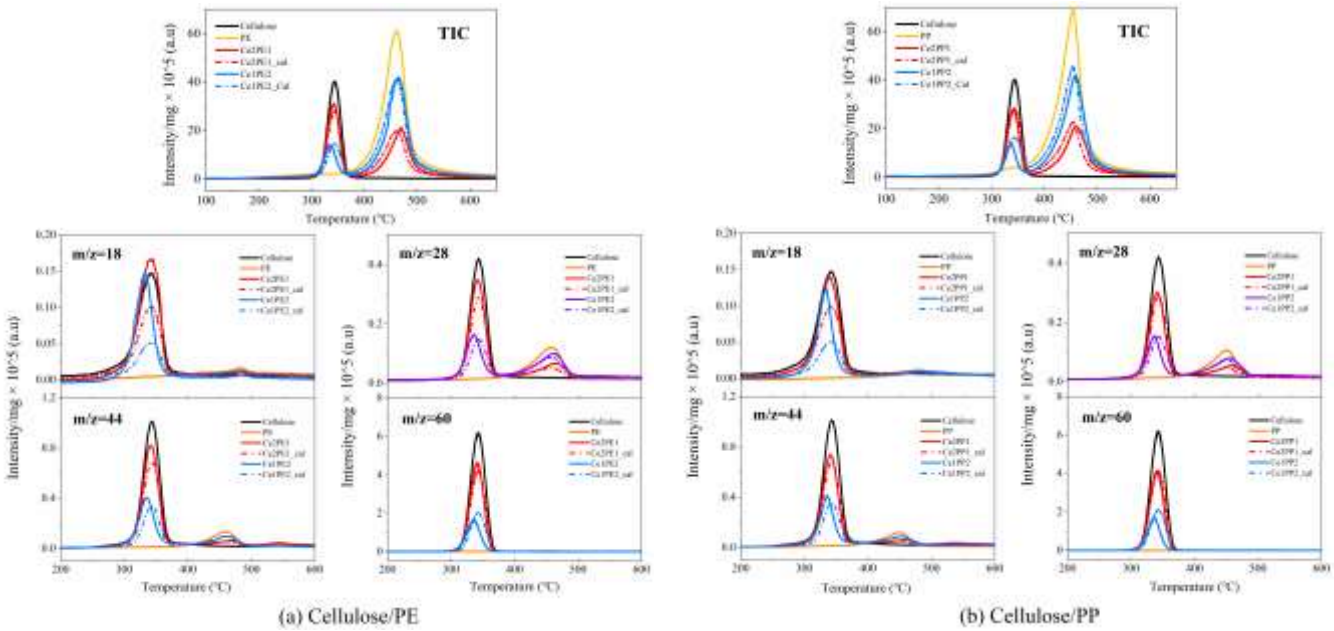

Fig. 6 Temperature-dependent product-emission behavior during the co-pyrolysis of (a) cellulose/PE and (b) cellulose/PP.

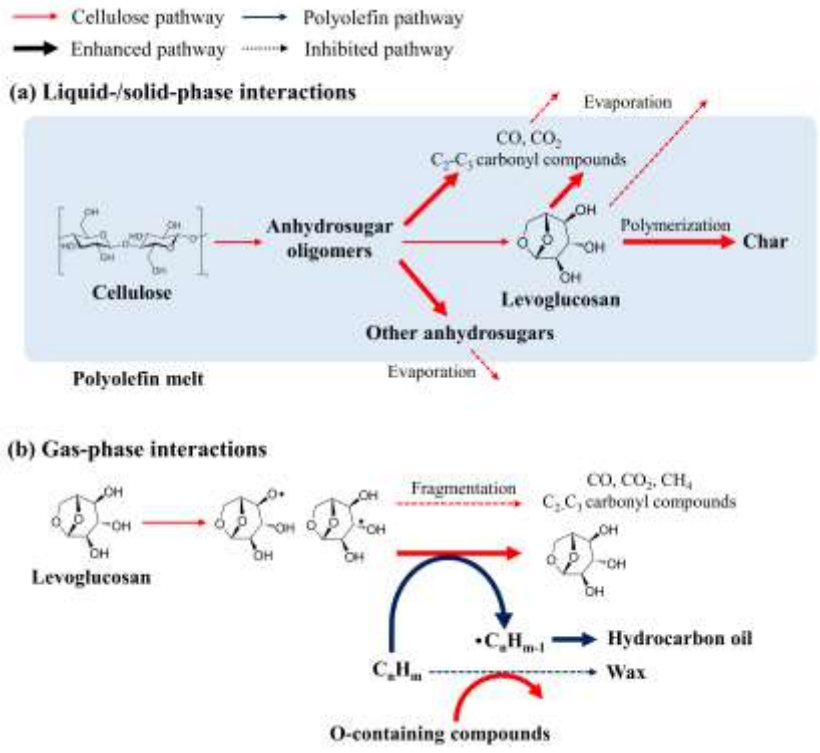

Fig. 7 Suggested pathways involving pyrolytic interactions between cellulose and polyolefins in (a) the liquid/solid phase and (b) the gas phase.